Error Reduction in Parameter Estimation from the Segmented Intravoxel Incoherent Motion Bi-exponential Model

Luis Agulles-Pedros[1], John L. Humm[1,2], Evis Sala[2], Hebert A. Vargas[2], Yousef Mazaheri[1,2]

[1]*Department of Medical Physics, Memorial Sloan Kettering Cancer Center, New York, USA,* [2]*Department of Radiology, Memorial Sloan Kettering Cancer Center, New York, USA*

ABSTRACT

Purpose: The purpose of the study was to develop and evaluate a method aiming at reducing the estimation error of the intravoxel incoherent motion (IVIM) model parameters reduced-error IVIM (reIVIM) and to compare the estimated parameters to those measured using the conventional "segmented" IVIM (seIVIM) algorithm. **Materials and Methods:** The prospective clinical component of this study was approved by the Institutional Review Board; all patients signed informed consent. 10 patients who underwent pre-treatment magnetic resonance (MR) imaging between July 2014 and May 2015 at 3-Tesla as part of a prospective study of the effect of radiation treatment on IVIM parameters were included. Diffusion-weighted MR images at 17 b-values (0, 10, 40, 70, 90, 100, 110, 120, 170, 210, 240, 270, 390, 530, 620, 750, and 1000 s/mm^2) were acquired at 4–8 consecutive time points. Using pre-treatment data, IVIM parameters (pseudo-diffusion D^*, true diffusion D, and perfusion-fraction f) were estimated from tumor regions of interest using the seIVIM and reIVIM algorithms. The repeatability of IVIM parameters for each algorithm was evaluated through assessment of the coefficient of variation (CV). For simulated data, precision and accuracy were evaluated as a function of noise. **Results:** Differences in CV for D and f between seIVIM and reIVIM (mean ± standard deviation %: 5.95 ± 2.63 and 5.94 ± 2.78 for D and 13.26 ± 4.94 and 10.54 ± 3.83 for f, respectively) were not significant ($P = 0.99$ and $P = 0.18$ for D and f, respectively). Differences in CV for D^* and $f \times D^*$ between seIVIM and reIVIM (40.88 ± 14.80% and 20.51 ± 7.71% for D^* and 45.10 ± 13.40% and 22.50 ± 8.48% for $f \times D^*$, respectively) were significant ($P = 0.0003$ and $P = 0.0003$ for D^* and $f \times D^*$, respectively). **Conclusion:** The proposed approach to the voxel-wise analysis of IVIM data results in the improved estimation of the pseudo-diffusion parameter by reducing the variability of the measurement.

Keywords: Diffusion-weighted magnetic resonance imaging, intravoxel incoherent motion, perfusion-fraction, pseudo-diffusion

INTRODUCTION

In biological tissue, the diffusion of water molecules is a complex phenomenon due to the heterogeneous microstructure of tissue as well as microperfusion within the capillary network. Le Bihan *et al*. proposed the intravoxel incoherent motion (IVIM) bi-exponential model to separate perfusion effects from pure diffusion in diffusion-weighted magnetic resonance imaging (DW-MRI) studies.[1-3] In this model, the signal intensity from a voxel is expected to decay in a bi-exponential fashion, which includes a rapid initial decrease due to the microvascular perfusion resulting in signal reduction at relatively low b-values, followed by a more gradual signal decrease due to tissue.

In the Le Bihan model for microvascular perfusion blood circulating through several thousand capillaries consisting

of "straight" segments oriented at various angles was modeled as a random, diffusion-like motion, with an effective diffusion coefficient.[2] Based on this model, the "diffusion" of blood within the capillaries depends on several factors, including vascular geometry and the rate of perfusion, and is much higher than the diffusion coefficient of tissue water.

Although it is more informative than the mono-exponential model, the IVIM model provides parameters that lack reproducibility to be reliable biomarkers.[4-6] Pekar *et al*. used computer simulations to study the precision and accuracy of bi-exponential parameters derived from multi-b-value DW experiments to characterize perfusion and diffusion.[4] Based on model parameter values for the brain, they generated a noise-contaminated signal at numerous signal-to-noise ratios (SNRs) and found that reliable estimates of perfusion coefficient, $D*$, and perfusion fraction, f, require substantial SNRs. The simulation also indicated that SNRs need to be higher for estimation of $D*$ than for f. The substantial SNRs required for reliable estimation of bi-exponential parameters could be achieved through averaging over regions of interest (ROIs). For voxel-wise analysis of IVIM diffusion parameters require more robust and reliable parameter estimation methods.

Several approaches have been presented in the literature to improve the reliability of the estimated IVIM parameters. One standard approach is the "segmented" IVIM (seIVIM) bi-exponential fitting.[7,8] In this approach, rather than simultaneously fitting data from all b-values, the data are divided into high- and low b-value ranges, and the IVIM parameters are estimated consecutively. Others have used alternative fitting approaches, including a Bayesian-Probability-based approach,[9,10] a Trust-Region-based algorithm,[11] and a fixed-$D*$ algorithm.[12,13] For a summary and comparison of different fitting strategies refer to Barbieri *et al*.[11]

The accurate and reliable assessment of bone marrow perfusion can provides valuable clinical information regarding tumor response to therapy as well as evaluation of compression fractures and metastasis.[14,15] Previous studies have used contrast-enhanced kinetics to evaluate tumor responses to radiotherapy in spinal bone metastases and to evaluate response to metastatic bone lesions.[16]

In this work, a simple method to improve data reliability of IVIM parameters, referred to as the reduced-error IVIM (reIVIM) estimation is presented. The method is based on the selection of pixels, which fulfill two conditions in each fitted parameter: (i) The parameter is within physiologically meaningful limits and (ii) the goodness-of-fit (GOF) of the estimation is within a predefined threshold. Voxels that do not meet the inclusion criteria are excluded from the analysis.

Using both simulation and human data the results are compared with the seIVIM, which does not pre-select voxels.

Theory
IVIM bi-exponential model

The bi-exponential IVIM model can be obtained by signal decay fitting of the following equation:

$$\frac{S(b)}{S(0)} = (1-f)ne^{-bnD} + fne^{-bnD} \tag{1}$$

Where $S(b)$ and $S(0)$ are signal intensities of each voxel with and without diffusion weighting, and the quantity, b, is the diffusion sensitizing factor (commonly referred to as the b-value). D is the diffusion coefficient, f is the volume fraction of water in perfused capillaries, and the pseudo-diffusion coefficient, $D*$, is dependent on the mean path length and blood velocity within the capillary network.

seIVIM bi-exponential fitting

Conventional seIVIM bi-exponential fitting is based on a 2-step fitting procedure; during the first step, the contribution from perfusion to the diffusion coefficient is ignored (as the one observed when high b-values larger than 200 mm²/s are applied) and the signal will follow:

$$\frac{S(b>200)}{S(0)} = e^{-bnD} \tag{2}$$

The perfusion fraction arises from the difference between the portion of the signal of those nuclei related to the intra- and extra-cellular diffusion, and the portion from those related to the microcirculation in the capillary network. Thus, f is obtained from the intercept of the linear regression of the logarithmic slope as:

$$f = 1 - \frac{S_{int}}{S(0)} \tag{3}$$

Where S_{int} is the intercept of the fitting of Eq. 2. The second step calculates $D*$ by fitting the exponential decay using a partially constrained nonlinear regression algorithm based on Eq. 1.

reIVIM bi-exponential fitting

A flow chart describing the algorithm is shown in Figure 1. In reIVIM segmented bi-exponential fitting, two exclusion criteria were included in the selection of voxels to be included in the final analysis. First, only voxels that have estimated values, which are within a certain pre-defined range of values, were included. These values were identified based on literature values and were deemed to be within the range of physiologically acceptable values. Voxels with parameters whose values exceed a pre-defined range are excluded from

the analysis. Second, voxels are excluded from the analysis if the estimation of the GOF of the residuals is below pre-defined values. Two exclusion criteria are applied systematically within the general framework of seIVIM. First, for *D* estimate, the physiological bounds as well as the GOF for the linear fit of logS(*b*) versus b for higher b-values (b-values >200 s/mm²) are incorporated. Only voxels that meet these criteria are further evaluated for estimation of *f*. Next, voxels with *f* values (estimated from Equation 3) that are within physiological bounds are included in the next phase of the analysis. Finally, for the subset of voxels that meet both the *D* and *f* criteria, the GOF criteria of the small b-values fitting applied to Equation 1 as well as the physiological bounds criteria for *D** are applied to identify the set of voxels that meet all the criteria required for estimation *D**.

Using the MATLAB® (version R2014b, The MathWorks, Inc., Natick, MA, USA) routine nlinfit.m for nonlinear regression algorithm, it is possible to estimate the four coefficients: The initial signal intensity S_0, *D*, *f*, and *D**. This fitting algorithm also returns residuals that can provide an estimate of the GOF. The maximum absolute error (MAE) is selected as the GOF criteria based on the simulation findings, which showed that it provided a robust metric to evaluate data fitting quality with reduced bias in the estimated parameters.

MATERIALS AND METHODS

Simulations
Monte Carlo simulations were performed to provide an improved understanding of the experimental findings and to determine confidence in the parameters derived from the IVIM estimations. Ideal signal intensity data were generated with the same 17 b-values used in the study: 0, 10, 40, 70, 90, 100, 110, 120, 170, 210, 240, 270, 390, 530, 620, 750, and 1000 s/mm². The simulations were performed assuming that the *in vivo* signal is biexponential, with parameters set to $f = 0.14 \pm 0.06$, $D = 0.60 \pm 0.09 \times 10^{-3}$ mm²/s, and $D* = 28 \pm 9 \times 10^{-3}$ mm²/s [Table 1]. The values were selected based on values reported by Marchand *et al*. for vertebral bone marrow using a non-negative least square algorithm[17] [Table 2]. To estimate the measurement errors induced by random noise, Rician-corrupted data were generated based on a method of Wiest-Daesslé *et al*.[18] 10,000 simulations were performed at each of the SNR levels: 9, 15, 23, 48, and 63. Precision and accuracy for each model were calculated. The precision of each parameter was characterized by its coefficient of variation (CV), defined as the ratio of the parameter's standard deviation (SD) to its mean. Accuracy was assessed by the relative bias, defined as the percentage difference between the fitted and ideal parameter values.

Patient selection
The prospective clinical component of this study was approved by the Institutional Review Board; all patients signed informed consent. Inclusion criteria were: (i) Histologically proven metastatic disease; (ii) patient deemed clinically appropriate for radiation treatment; (iii) life expectancy >6 months; and (iv) age ≥18 years. Exclusion criteria were: (i) Inability to give informed consent; (ii) inability to comply with the protocol, (iii) contraindications to MRI; (iv) tumors involving visceral organs, brain or spinal cord; (v) platelet count <75,000/µl, hemoglobin level <9 g/dl, white blood count <3500/µl; (vi) metastases in the upper thoracic spine (to avoid MRI artifacts due to cardiac motion); and (vii) lesions <1.5 cm (to ensure robust measurements thereby avoiding potential issues due to limited spatial resolution).

All patients underwent MRI before radiation therapy on a 3 Tesla MR scanner (MR750, GE Healthcare, Wisconsin, USA). DW-MRI was acquired at 4–8 consecutive time points with 4-min intervals between acquisitions. A body coil was used for excitation. For signal reception, the vendor's standard 6-element
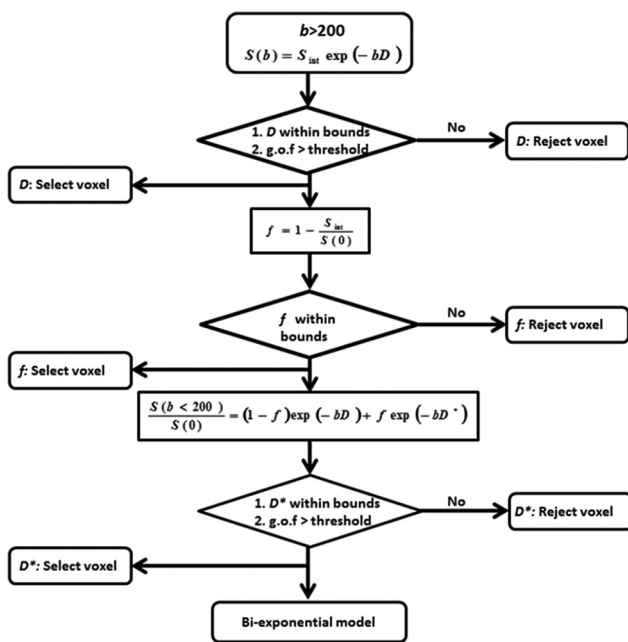

Figure 1: Flow diagram for pixel selection to analyze each intravoxel incoherent motion parameter

Table 1: IVIM parameters used in the simulations. The mean values were based on the non-negative least square algorithm reported for vertebral bone marrow.[17] The range was set to 2×SD of the literature values from Table 2

Parameter	Tumor mean	Tumor, range (minimum, maximum)
D, (10⁻³ mm²/s)	0.60	(0.23, 0.97)
f, (%)	14	(1.30, 26.71)
*D**, (10⁻³ mm²/s)	28	(9.07, 65.86)

IVIM: Intravoxel incoherent motion, SD: Standard deviation

spine phased array coil was used, allowing simultaneous operation of four of the six array coils and reconstruction of a sum-of-squares image from the four intermediate coil MR images. DW images were obtained using a Stejskal-Tanner pulsed gradient spin echo sequence and spin-echo echoplanar imaging readout. Multi b-value DW MRI (b = 0, 10, 40, 70, 90, 100, 110, 120, 170, 210, 240, 270, 390, 530, 620, 750, and 1000 s/mm²) was acquired using the following parameters: TR/TE = 2200/80.2 ms, number of averages = 2, matrix 128 × 128, field of view 320 × 160 mm², and spatial resolution 2.5 × 1.25 × 5 mm³, with an acceleration factor of 2. The acquisition was repeated 16 times. Conventional T_1- and T_2-weighted MR images were also acquired for anatomical correlation, using an existing standard of care clinical protocol. Volumes of interest covering lesions were outlined by experienced MRI radiologists on apparent diffusion coefficient maps, using a combination of the T_1-weighted and DW-MR images for guidance. MR image post-processing was performed using in-house software written in MATLAB (version R2014b, The MathWorks, Inc., Natick, MA, USA).

Data analysis

After selection of original and selected pixels D, f, and D^*, the average of each parameter and CV was computed. In the case of simulations, accuracy and bias were calculated. The Wilcoxon signed-rank test was used to analyze differences between pre- and post-contrast parameters. Scatter-plots and the Pearson correlation coefficient were used to quantify the relationships between variables. A value of $P < 0.05$ was accepted as the minimum level of significance.

RESULTS

Figure 2a is the mean estimated D^* as a function of MAE from a patient data. The estimation of D^* is 27×10^{-3} mm²/s when MAE threshold of 0.4 is used compared with 27×10^{-3} mm²/s at MAE = 1. Figure 2b is the percentage of voxels used as a function of MAE. At MAE = 0.4, 38% of the voxels are included in the analysis. Based on the empirical evaluation of all patient data, a MAE threshold of 0.5 was selected.

Simulations show comparison of bias [Figure 3a] and CV [Figure 3b] for seIVIM and reIVIM algorithms. For SNR = 9, the bias in D^* was −53.30% for seIVIM and −4.70% for reIVIM. For higher SNR, there were fewer improvements. For SNR = 35, the bias in D^* was −1.35% for seIVIM and −0.87% for reIVIM.

| Table 2: Literature values for bone marrow IVIM parameters				
Literature values	**Description**	**D, (10^{-3}mm²/s)**	**f, (%)**	**D^*, (10^{-3}mm²/s)**
Marchand *et al*.[17]	Vertebral bone marrow using non-negative least square algorithm	0.60±0.09	14±6	28±9
	Vertebral bone marrow using Levenberg-Marquardt algorithm	0.45±0.27	27±17	63±145
Niu *et al*.[21]	Acute myeloid leukemia before treatment (complete responders)	0.24±0.04	22.38±5.19	67.22±7.07
	Acute myeloid leukemia before treatment (non-responders)	0.20±0.03	27.89±8.25	66.80±6.76

IVIM: Intravoxel incoherent motion
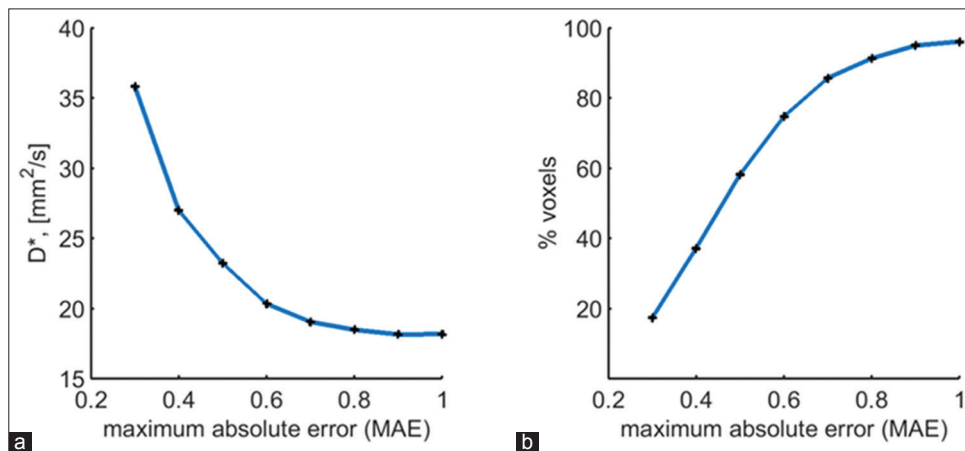
Figure 2: (a) Mean estimated D^* as a function of maximum absolute error (MAE) from a patient data. (b) Percentage of voxels used as a function of MAE. Based on the empirical evaluation of all patient data, a MAE threshold of 0.5 was selected

A representative plot of the mean signal from an ROI using seIVIM and reIVIM is shown in Figure 4. Importantly, the mean (±SD) value of $D*$ is 20.47 ± 4.24 mm²/s when conventional (seIVIM) as compared with 29.89 ± 4.60 mm²/s if the reIVIM method was employed Also shown is the magnified region for b-values 0–300 s/mm². Table 3 shows the mean *in vivo* measurements data for all 10 patients. Figure 5 shows the selection criteria from a slice through the center of the tumor for each of the three parameters (D, f, and $D*$) for all 10 patients and shows the three steps in the selection process. Usually, voxels meet the criteria for D. The perfusion fraction criteria provided a substantial threshold to voxel selection that was further refined by the $D*$ criteria. For example, for patient 5, the percentage of selected voxels for the reIVIM is 99.40% in D, 89.70% in f, and 60.55% in $D*$. The parametric maps for patient 5 are shown in Figure 6.

In Table 4, the CV of the fitted values for the two methods is compared. A significant improvement (reduction in CV values) in the estimation of $D*$ ($P = 7.68 \times 10^{-4}$) and $f \times D*$ ($P = 1.1 \times 10^{-3}$) was observed when seIVIM and reIVIM were compared. The CV of D and f were not significantly different for the two methods ($P = 0.88$ and $P = 0.10$, respectively). A box-plot representation is shown in Figure 7.

The dependence of the CV of the perfusion-related parameters f, $D*$, and $f \times D*$ was evaluated as a function of f [Figure 8]. Based on the slopes of the fitted lines, there is no noticeable change when seIVIM and reVIM methods are compared for f (slopes were −0.3 in both cases). For $D*$ and $f \times D*$, the slopes were substantially different for the two methods (−1.4 and −1.5 for seIVM as compared with −0.4 in both cases for reIVIM, respectively).

DISCUSSION

A method has been presented to improve the bias and precision of the fitted IVIM parameters that rely on the inclusion of voxels, which satisfy pre-defined inclusion
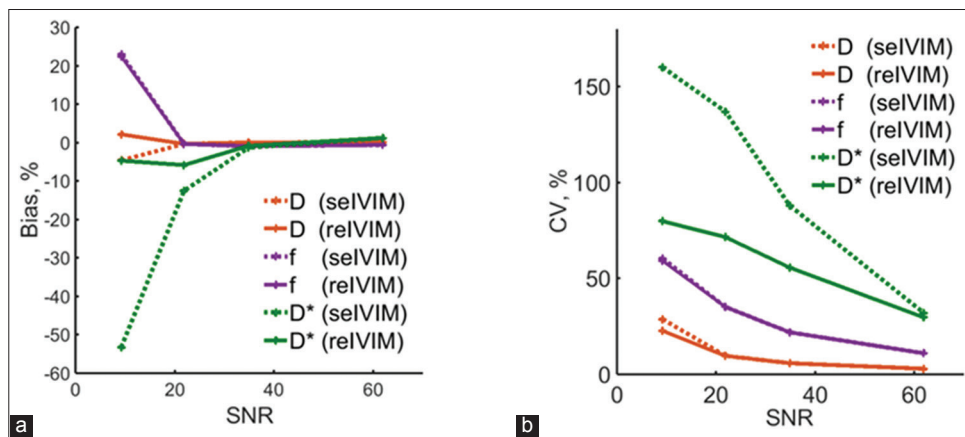
Figure 3: Monte Carlo simulations of accuracy (bias) (a) and precision (coefficient of variation) (b) of D, f, and $D*$ parameters versus signal-to-noise ratio
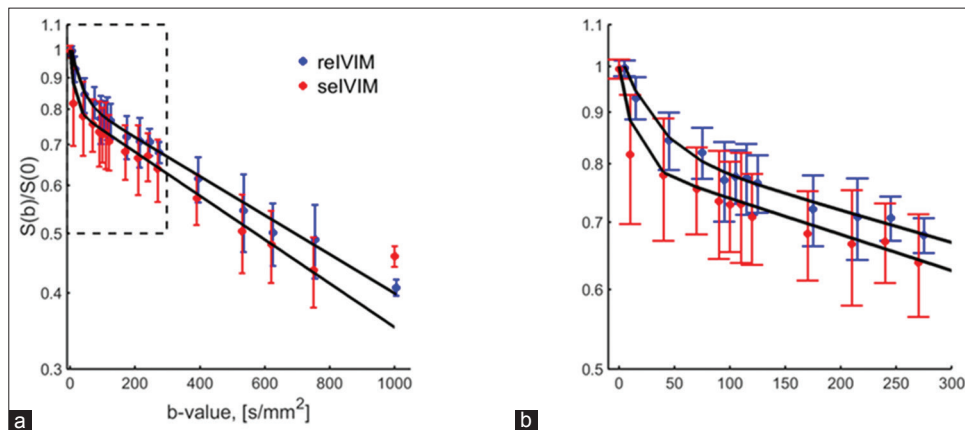
Figure 4: Representative plot of the mean signal from a region of interest using "segmented" intravoxel incoherent motion (seIVIM) and reduced-error intravoxel incoherent motion (reIVIM). The mean (±standard deviation) value of D, f, and $D*$ was 6.86±0.42 mm²/s, 17.03±1.84%, and 20.47±4.24 mm²/s, respectively, when conventional (seIVIM) as compared with 17.03±1.84 mm²/s, 17.05±1.81%, and 29.89±4.60 mm²/s, respectively, if the reIVIM method was employed
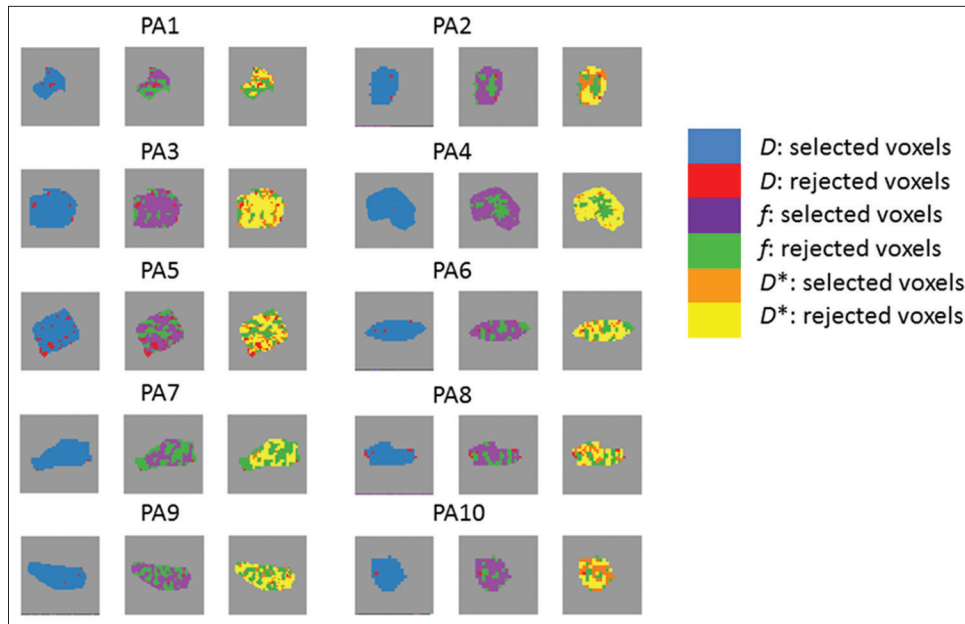
Figure 5: Selection criteria from a slice through the center of the tumor for each of the three parameters (*D, f,* and *D**) for all 10 patients

Table 3: Mean (minimum, maximum) of median (overall voxels) *D, f, D** and *f×D** for the patient population			
Parameter	**selVIM**	**relVIM**	***P***
D, (10⁻³ mm²/s)	0.71 (0.33,1.39)	0.71 (0.33,1.39)	1.0
f, (%)	13.33 (6.32,24.97)	13.84 (6.4,25.54)	0.62
D*, (10⁻³ mm²/s)	8.81 (4.73,20.47)	30.27 (10.03,46.64)	3.3×10⁻⁴*
F×D*, (10⁻³ mm²/s)	1.28 (0.46,3.49)	4.28 (0.64,6.99)	0.0073*

selVIM: "Segmented" intravoxel incoherent motion, relVIM: Reduced-error intravoxel incoherent motion

Table 4: Mean values of CV of the fitted values throughout the 10 patients. The asterisk indicates significance (Wilcoxon rank-sum test *P* value <0.05)			
Parameter	**selVIM**	**relVIM**	***P* %**
CV of *D* (%)	5.95±2.63	5.94±2.78	0.88
CV of *f* (%)	13.26±4.94	10.54±3.83	0.10
CV of *D** (%)	40.88±14.80	20.51±7.71	7.68×10⁻⁴*
CV of *f×D** (%)	45.10±13.40	22.50±8.48	1.1×10⁻³*

selVIM: "Segmented" intravoxel incoherent motion,
relVIM: Reduced-error intravoxel incoherent motion,
CV: Coefficient of variation

criteria. The approach has been evaluated on both simulated data and *in vivo* human data.

Selection criteria were key to achieving improvements in data robustness. The criteria that have been incorporated consider boundary conditions of the estimated parameters as well as a metric that assesses the GOF of the fitting processes. By applying these selection criteria, improved fitting of the voxels which exclude voxels that do not meet the requirements of our model has been achieved.

Spatial maps to display the selection process have been generated. The maps are also beneficial because they could provide localization of regions within a tumor that are, for example, perfusion deficient, due to necrosis. The approach of mapping error for the analysis of pharmacokinetics data was previously proposed by Gill *et al*.[19] Here, their approach has been extended to the analysis of IVIM data.

The quality of the simulated fitted parameters was assessed in terms of precision and bias, which showed a strong dependence on SNR. However, *in vivo* data can offer a wide range of SNR within the ROI, implying that the benefits of the approach could vary. Overall, a significant improvement was found in CV of *D** (as well as the product of *f, D**, and *f × D**), which was consistent with our findings from simulations in the range of SNR = 10–30. The parameter *D* was highly reproducible, and the CV did not significantly change with the proposed method. There was an improvement in the CV
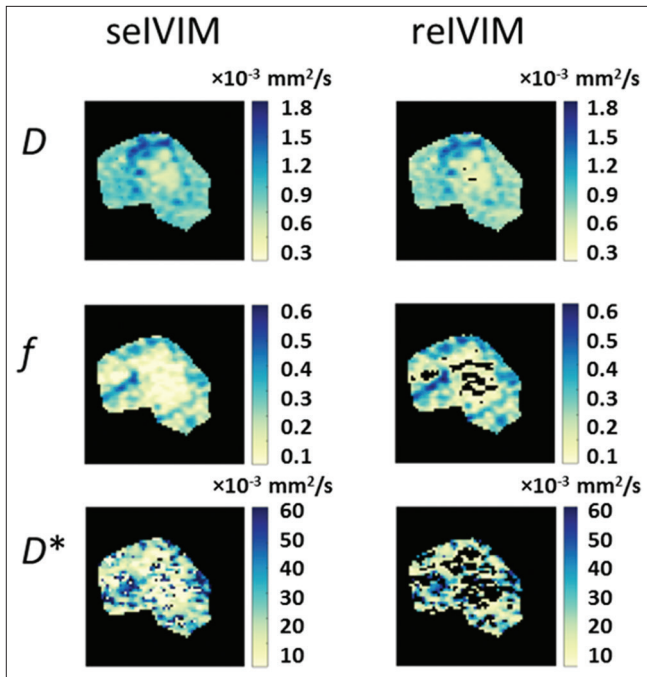
Figure 6: Parametric maps of *D*, *f*, and *D** based on "segmented" intravoxel incoherent motion and reduced-error intravoxel incoherent motion for patient 5

of *f*, though it did not reach the level of statistical significance ($P = 0.10$). The simulations suggest a substantial bias in *D** in the SNR range of 10–30, which is reduced drastically with the reIVIM method. From the *in vivo* data [Table 3], a significant increase was found in estimated *D**. The trend is consistent with the reduction in bias observed from the simulation results. There were no significant changes in the estimated values of *D* and *f* when the reIVIM method was applied as compared with the seIVIM method. This trend was also consistent with the simulation results.

A limitation of measuring microperfusion related parameters using IVIM is the relatively small contribution to the signal from the capillary compartment as given by *f*. Hence, the relationship between perfusion fraction, *f*, and the CV of the perfusion-related parameters (*f*, *D**, and $f \times D^*$) has been explored. The results [Figure 8] suggest that in the estimation of *D** (and $f \times D^*$) with the standard method (seIVIM), the CVs are sensitive to the value of *f* (due to the higher negative slope of seIVIM). For reIVIM, the slope is substantially lower, which implies that the CV for the proposed method is less dependent on the value of *f*. The slope of CV (*f*) does not appear to change when comparing the two methods, though reIVIM has reduced CV at all *f* values as compared with seIVIM.
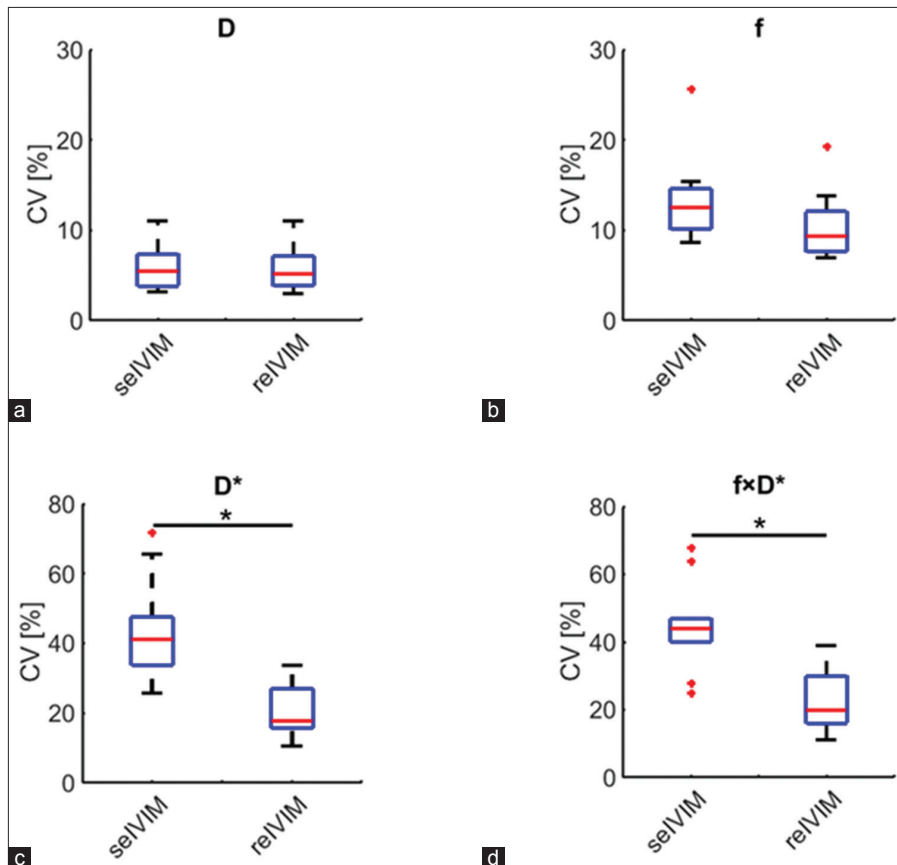

Figure 7: Box-and-whisker plots of variation (coefficient of variation) of (a) *D*, (b) *f*, (c) *D**, and (d) *f×D** for the "segmented" intravoxel incoherent motion (seIVIM) and reduced-error intravoxel incoherent motion (reIVIM) methods. Red lines median values; bottom of box, 25 percentile; top of box, 75th percentile. Kruskal–Wallis test demonstrated statistical significance for differences between the seIVIM and reIVIM methods
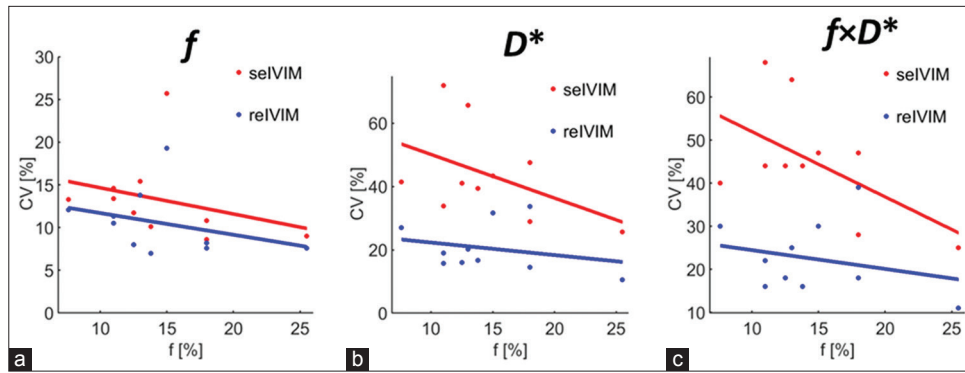
Figure 8: Coefficient of variation (CV) of the perfusion-related parameters *f*, *D**, and *f*×*D** versus *f* for the "segmented" intravoxel incoherent motion (seIVM) and reduced-error intravoxel incoherent motion (reIVIM) methods. A linear regression of both sets of data is shown (solid line). For seIVIM and reVIM methods, the slopes for CV (*f*) versus *f* were −0.3±0.3 in both cases. For CV (*D**) versus *f*, the slopes were −1.4±0.9 and −0.4±0.5 for the seIVIM and reVIM methods, respectively. For CV (*f*×*D**) versus *f*, the slopes were −1.5±0.8 and −0.4±0.6 for the seIVIM and reVIM methods, respectively

The standard monoexponential diffusion model provides a reliable estimate of diffusion coefficient, namely the apparent diffusion coefficient. However, an extension of this model to those models that incorporate micro-perfusion (such as IVIM) or restricted diffusion (such as the non-Gaussian diffusion kurtosis model)[20] is often limited by the reduced reliability of the estimated parameters. The approach presented here can be extended to other diffusion models (including the non-Gaussian diffusion kurtosis model), providing a tool for more robust analysis of diffusion parameters.

The present study had some limitations. A major limitation of this study is the small sample size. Second, because the source of the error beyond low SNR has not been examined, the question of whether the method can be used to identify regions of low blood perfusion has not been addressed. An additional source of error is motion, or fat signal, contamination, which was not incorporated in the analysis. Additional studies will need to incorporate the contribution from these and other sources to increase the reliability of IVMI parameters.

CONCLUSION

We have proposed an approach to the voxel-wise analysis of IVIM data that results in the improved estimation of the pseudo-diffusion parameter by reducing the variability of the measurement.

ACKNOWLEDGMENTS

REFERENCES

1. Le Bihan D, Turner R, MacFall JR. Effects of intravoxel incoherent motions (IVIM) in steady-state free precession (SSFP) imaging: Application to molecular diffusion imaging. Magn Reson Med 1989;10:324-37.
2. Le Bihan D, Breton E, Lallemand D, Grenier P, Cabanis E, Laval-Jeanet M, *et al*. MR imaging of intravoxel incoherent motions: Application to diffusion and perfusion in neurologic disorders. Radiology 1986;161:401-7.
3. Le Bihan D, Breton E, Lallemand D, Aubin ML, Vignaud J, Laval-Jeanet M, *et al*. Separation of diffusion and perfusion in intravoxel incoherent motion MR imaging. Radiology 1988;168:497-505.
4. Pekar J, Moonen CT, van Zijl PC. On the precision of diffusion/perfusion imaging by gradient sensitization. Magn Reson Med 1992;23:122-9.
5. King MD, van Bruggen N, Busza AL, Houseman J, Williams SR, Gadian DG, *et al*. Perfusion and diffusion MR imaging. Magn Reson Med 1992;24:288-301.
6. Riches SF, Hawtin K, Charles-Edwards EM, de Souza NM. Diffusion-weighted imaging of the prostate and rectal wall: Comparison of biexponential and monoexponential modelled diffusion and associated perfusion coefficients. NMR Biomed 2009;22:318-25.
7. Chandarana H, Lee VS, Hecht E, Taouli B, Sigmund EE. Comparison of biexponential and monoexponential model of diffusion weighted imaging in evaluation of renal lesions: Preliminary experience. Invest Radiol 2011;46:285-91.
8. Freiman M, Voss SD, Mulkern RV, Perez-Rossello JM, Callahan MJ, Warfield SK, *et al*. *In vivo* assessment of optimal b-value range for perfusion-insensitive apparent diffusion coefficient imaging. Med Phys 2012;39:4832-9.
9. Neil JJ, Bretthorst GL. On the use of bayesian probability theory for analysis of exponential decay data: An example taken from intravoxel incoherent motion experiments. Magn Reson Med 1993;29:642-7.
10. Dyvorne HA, Galea N, Nevers T, Fiel MI, Carpenter D, Wong E, *et al*. Diffusion-weighted imaging of the liver with multiple b values: Effect of diffusion gradient polarity and breathing

acquisition on image quality and intravoxel incoherent motion parameters–a pilot study. Radiology 2013;266:920-9.

11. Barbieri S, Donati OF, Froehlich JM, Thoeny HC. Impact of the calculation algorithm on biexponential fitting of diffusion-weighted MRI in upper abdominal organs. Magn Reson Med 2016;75:2175-84.

12. Heusch P, Wittsack HJ, Pentang G, Buchbender C, Miese F, Schek J, *et al.* Biexponential analysis of diffusion-weighted imaging: Comparison of three different calculation methods in transplanted kidneys. Acta Radiol 2013;54:1210-7.

13. Wittsack HJ, Lanzman RS, Mathys C, Janssen H, Mödder U, Blondin D, *et al.* Statistical evaluation of diffusion-weighted imaging of the human kidney. Magn Reson Med 2010;64:616-22.

14. Chen WT, Shih TT, Chen RC, Lo HY, Chou CT, Lee JM, *et al.* Blood perfusion of vertebral lesions evaluated with gadolinium-enhanced dynamic MRI: In comparison with compression fracture and metastasis. J Magn Reson Imaging 2002;15:308-14.

15. Fenchel M, Konaktchieva M, Weisel K, Kraus S, Brodoefel H, Claussen CD, *et al.* Early response assessment in patients with multiple myeloma during anti-angiogenic therapy using arterial spin labelling: First clinical results. Eur Radiol 2010;20:2899-906.

16. Chu S, Karimi S, Peck KK, Yamada Y, Lis E, Lyo J, *et al.* Measurement of blood perfusion in spinal metastases with dynamic contrast-enhanced magnetic resonance imaging: Evaluation of tumor response to radiation therapy. Spine (Phila Pa 1976) 2013;38:E1418-24.

17. Marchand AJ, Hitti E, Monge F, Saint-Jalmes H, Guillin R, Duvauferrier R, *et al.* MRI quantification of diffusion and perfusion in bone marrow by intravoxel incoherent motion (IVIM) and non-negative least square (NNLS) analysis. Magn Reson Imaging 2014;32:1091-6.

18. Wiest-Daesslé N, Prima S, Coupé P, Morrissey SP, Barillot C. Rician noise removal by non-local means filtering for low signal-to-noise ratio MRI: Applications to DT-MRI. Med Image Comput Comput Assist Interv 2008;11:171-9.

19. Gill AB, Anandappa G, Patterson AJ, Priest AN, Graves MJ, Janowitz T, *et al.* The use of error-category mapping in pharmacokinetic model analysis of dynamic contrast-enhanced MRI data. Magn Reson Imaging 2015;33:246-51.

20. Jensen JH, Helpern JA, Ramani A, Lu H, Kaczynski K. Diffusional kurtosis imaging: The quantification of non-gaussian water diffusion by means of magnetic resonance imaging. Magn Reson Med 2005;53:1432-40.

21. Niu J, Li W, Wang H, Wu W, Gong T, Huang N, *et al.* Intravoxel incoherent motion diffusion-weighted imaging of bone marrow in patients with acute myeloid leukemia: A pilot study of prognostic value. J Magn Reson Imaging 2017;46:476-82.